The LISA DFACS: effects of micrometeoroid impacts in the drag-free mode

The LISA DFACS: effects of micrometeoroid impacts in the drag-free mode

occurs, the constellation acquisition procedure must be repeated, which consists in performing a time-consuming scanning spiral to search for the other spacecrafts. Another issue is related to the fact that the relative attitude and position perturbation between the spacecraft and the test masses could be so high that the latter escape from the electrostatic control. When this occurs, it is necessary to re-grab the test masses by switching the operating mode of the electrostatic suspensions to Wide Range Mode This switch increases the actuator authority levels as well as the sensing ranges and noise levels compared to the High Resolution Mode used in drag free.

In this paper, the micrometeoroid issue is addressed. The effects of impacts with different intensities acting on the surface of a LISA spacecraft is evaluated. It is observed that in case of strong impacts, the attitude perturbation is such that the laser beams can actually exceed the receiving sensor range. Hence, a control strategy for a fast recovery of the constellation without performing a scanning spiral is designed. In particular, a detector based on a state observer detects the impact and changes the operating mode from drag-free to recovery mode. The guidance and the controller are changed accordingly. In this paper, the mathematical model of micrometeoroid impacts and their effects on a LISA spacecraft running drag-free mode are developed. Then, the adopted control design approach for the recovery mode is presented. Finally, simulation results are shown, demonstrating the effectiveness of the proposed approach.

2. Methodology

The LISA system has been simulated by means of a nonlinear model developed in a precedent work [1], implemented on Simulink. This simulator includes all the sensor and actuator noises used during the main science phase of the mission. Also, it takes into consideration external disturbances such as the solar pressure and the gravity force generated by the spacecraft on the test masses (self-gravity). The control system shown in [2] is already implemented in the simulator.

For this work, the simulator has been extended to include the micrometeoroid impacts that affect the spacecraft dynamics, and the recovery control system designed in this paper.

In addition, a high-fidelity simulator developed by Thales Alenia Space has been used to perform the final Monte Carlo campaign. This simulator also includes, among other things, the scheduling of the commands to the 9 independent thruster composing the MPS system and their dynamics.

3. Micrometeoroid Impacts

A Micrometeoroid is an extremely small particle of rock, that usually weighs less than a gram. During their orbits, the LISA spacecraft may frequently encounter streams of micrometeoroids, causing multiple impacts. The data on these impacts has been provided by the European Space Agency.

In the simulator, meteoroid impacts are modeled using rectangular force and torque impulses of short duration that account for the linear and angular momenta transferred during the collision.

3.1. Impact data analysis

The impact dataset provided by ESA consists in 219728 impacts, each described by the following features:

1. particle linear momentum **p**: the norm of the linear momentum of the particle;
2. transferred linear momentum $\boldsymbol{p}_i$: the linear momentum transferred to the SC during impact, along each axis;
3. transferred angular momentum $\mathbf{H}_i$: the angular momentum transferred to the SC during impact, along each axis;
4. speed variation Δv : the variation in the norm of the particle's speed due to impact;
5. angular speed variation $\Delta\omega$: the variation in the norm of the particle's angular speed due to impact;
6. Impact Point $\boldsymbol{r}_i$: the impact point on the outer surface of the Spacecraft.

The main quantities affecting the SC are the transferred linear and angular momenta. These features span several order of magnitude, for this reason the impacts were first grouped using this criteria. Different signs are treated as different groups. Table 1 reports them in detail.

Table 1. Impact grouping by order of magnitude of transferred momenta

Id	Range
G_7^-	$[-10^{-2}; -10^{-3})$
G_6^-	$[-10^{-3}; -10^{-4})$
G_5^-	$[-10^{-4}; -10^{-5})$
G_4^-	$[-10^{-5}; -10^{-6})$
G_3^-	$[-10^{-6}; -10^{-7})$
G_2^-	$[-10^{-7}; -10^{-8})$
G_1^-	$[-10^{-8}; -10^{-9})$
G_0	$[-10^{-9}; 10^{-9}]$
G_1	$(10^{-9}; 10^{-8}]$
G_2	$(10^{-8}; 10^{-7}]$
G_3	$(10^{-7}; 10^{-6}]$
G_4	$(10^{-6}; 10^{-5}]$
G_5	$(10^{-5}; 10^{-4}]$

G_6	$(10^{-4}; 10^{-3}]$
G_7	$(10^{-3}; 10^{-2}]$

As shown in Figure 1, most of the transferred momenta are in the range of group G_0, that represents orders of $\pm 10^{-10}$ or smaller. These are very low-energy impacts and do not cause any stability issues. Figure 2 shows, on a group basis, the percentage distribution on the three x, y and z axis. A few remarks can be drawn:

1. most of the stronger hits in the negative ranges (groups G_7^- to G_0) transfer the linear momentum along the -z direction, this is mainly due to the wide solar panel on the top of the Spacecraft (area ≈ 13.5 m^2);
2. among the stronger hits in the positive ranges (groups G_0 to G_7^+ the linear momentum transfers are more evenly spread out, even if a slight preference for the +z direction can be observed for the most powerful impacts (group G_7^+);
3. most of the stronger impacts transfer angular momentum along the x axis, this again is due to the long rectangular solar panel, that when hit on the border furthest from the SC's CoM offers a long rotation arm to the meteoroid, exerting higher torques on the SC's x axis.

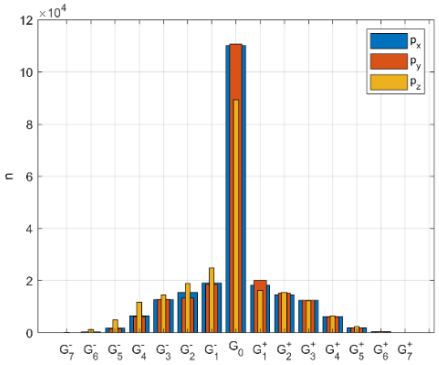

(a) Transferred Linear Momentum

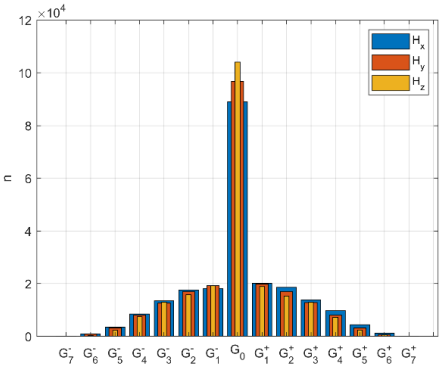

(b) Transferred Angular Momentum

Figure 1. Samples count for each impact group

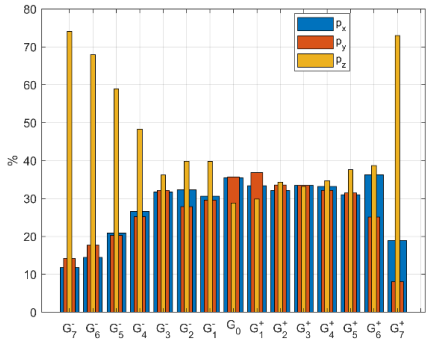

(a) Transferred Linear Momentum

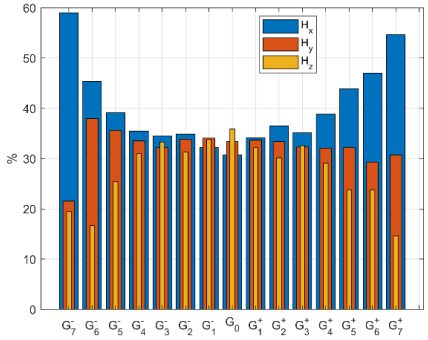

(b) Transferred Angular Momentum

Figure 2. Percentage distribution on the three axis for each group

3.2. Effects on the drag-free control

During the science phase of the LISA mission the main control system that is active is the drag-free and attitude control system.

As already stated in the introduction, micrometeoroid impacts may constitute a problem for the main drag-free controllers. Specifically, there are some impacts that have sufficient energy to cause a perturbation in the spacecraft's attitude that exceeds the maximum allowed angular pointing error of 2 μrad. An example of this can be seen in Figure 3b, that shows the azimuth and elevation angles of the incoming laser beams in each of the two optical units installed in each of the spacecraft. The angles of the incoming laser beams exceed the maximum allowed threshold of 2 μrad soon after the impact (in Figure 3 after 200 seconds). The impact shown is one of the strongest available in the dataset with $\boldsymbol{p}_i = [-2.54 \quad -0.93 \quad 14.94] \cdot 10^{-3}\, Ns$ and $\boldsymbol{H}_i = [-4 \quad -19.89 \quad 0.56] \cdot 10^{-3}\, Nms$. On the other hand, most of the impacts are less energetic and the drag-free controllers are able to keep the laser links within their operating range. An example of this case is shown in Figure 3a, where the impact is

characterized by $\boldsymbol{p}_i = [0.09 \quad 0.04 \quad 0.19] \cdot 10^{-3}\ Ns$ and $\boldsymbol{H}_i = [-0.4 \quad -0.07 \quad 0.22] \cdot 10^{-3}\ Nms$.

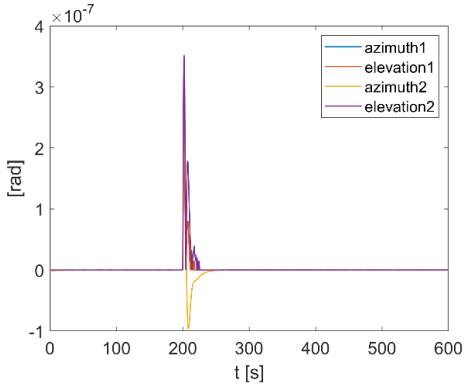

a) Low Energy Impact

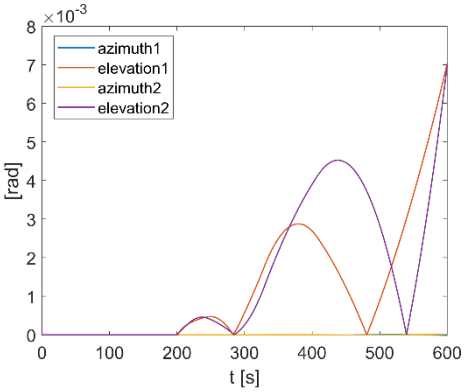

b) High Energy Impact

Figure 3. Laser beam angular deviations following a micrometeoroid impact

4. Recovery Mode Control Design

The proposed recovery control system allows for a fast laser link reacquisition, without needing the complete constellation acquisition, that may take several hours to be completed. Its general structure is shown in Figure 4. The impact detector is able to detect when an impact occurs by monitoring the spacecraft's measured state, appropriately extended by means of state observers, and to trigger a recovery signal. When the recovery signal is triggered the drag-free controllers for the spacecraft attitude and test masses positions are replaced by recovery controllers. The recovery guidance provides the reference spacecraft's inertial attitude to be tracked during the recovery maneuver.

4.1. Impact detector

The impact detector module is based on monitoring some components of the spacecraft's state. Specifically, it activates the recovery signal when at least one among the Euclidean norms of the signals of interest exceed their respective thresholds.

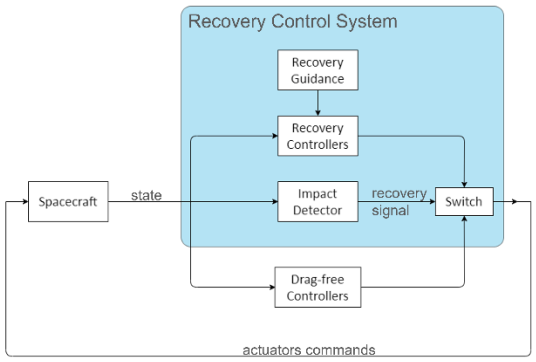

Figure 4. General architecture of the recovery system

The first considered signal is $\boldsymbol{\omega}_{SC}$ the first derivative of the spacecraft's attitude angular error $\boldsymbol{\theta}_{SC}$. The laser sensors directly measure the quaternion $\mathbf{q}_{SC}$ from which $\boldsymbol{\theta}_{SC}$ is easily obtained (quaternion to Euler321 conversion); whereas $\boldsymbol{\omega}_{SC}$ is obtained according to the following discrete-time equation:

$$\boldsymbol{\omega}_{SC}(k) = \left(\boldsymbol{\theta}_{SC}(k) - \boldsymbol{\theta}_{SC}(k-1)\right)\frac{1}{\tau} \qquad (1)$$

where k represents the discrete-time step and $\tau = 0.01$ s is the time interval of the numerical differentiator.

The other two considered signals are the positions of the two test masses with respect to the centers of their housings, respectively $\boldsymbol{r}_{m_1}$ and $\boldsymbol{r}_{m_2}$, that are directly measured by the electrodes positioned on the walls of the housings, as illustrated in Figure 5.

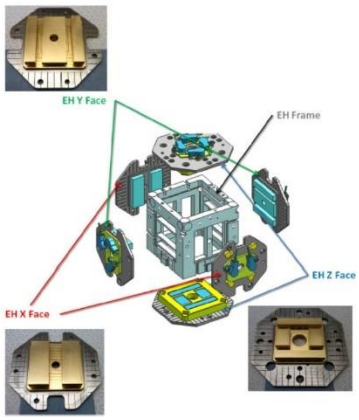

Figure 5. Test Mass housing with electrodes

The recovery signal is triggered when one of the following conditions becomes true:

- $\|\boldsymbol{\omega}_{SC}\|_2 > \bar{\omega}_{SC}$
- $\|\boldsymbol{r}_{m_1}\|_2 > \bar{r}_m$
- $\|\boldsymbol{r}_{m_2}\|_2 > \bar{r}_m$

The thresholds $\bar{\omega}_{SC}$ and $\bar{r}_m$ are scalar values tuned in order to reduce the impact detection time, that is the

time elapsed between the impact instant and the instant when the recovery signal is triggered, and to have zero false negatives, that are cases where the impact detector should have triggered the recovery signal but has not. This tuning has been performed by simulating all the impacts in the dataset that cause significant perturbation. The tuning found is $\bar{\omega}_{SC} = 3.36\,\mu\text{rad/s}$ and $\bar{r}_m = 5.45\,\mu\text{m}$.

In addition to the detection task, the impact detector also performs the end of recovery, that is, it determines when the system is near enough to the science mode working point to be ready to switch back to the drag-free controllers. This is also performed by a threshold-based strategy. More specifically, when the following conditions are all true at the same time then the system is switched back to science mode:

- $\left|2\cos^{-1} \mathrm{q}_{SC_0}\right| \leq \underline{\theta}_{SC}$
- $\|\boldsymbol{\omega}_{SC}\|_2 \leq \underline{\omega}_{SC}$
- $\left\|\boldsymbol{r}_{m_1}\right\|_2 \leq \underline{r}_m$
- $\left\|\boldsymbol{r}_{m_1}\right\|_2 \leq \underline{r}_m$

where q_{SC_0} is the scalar part of the quaternion $\mathbf{q}_{SC}$ that represents the attitude error of the spacecraft. The thresholds $\underline{\theta}_{SC}$, $\underline{\omega}_{SC}$, $\underline{r}_m$ are scalar values tuned to reduce the number of oscillations between drag-free and recovery mode at the end of recovery. The tuning found is $\underline{\theta}_{SC} = 2.1\ \mu\text{rad}$, $\underline{\omega}_{SC} = 2\ \mu\text{rad/s}$ and $\underline{r}_m = 3.56\,\mu\text{m}$.

4.2. State Machine

The operating mode of each spacecraft of the LISA system can be modeled by a state machine. During the science mode the system is in the first starting state S0. When an impact occurs, the system transitions into other states, depending on the intensity of the collision. The main properties of interest of the LISA system are

1. P1 spacecraft attitude convergence, with possible values convergent/divergent;
2. P2 test mass attitude convergence, with possible values convergent/divergent;
3. P3 test mass position convergence, with possible values convergent/divergent;
4. P4 incoming laser link loss, with possible values loss/no loss;
5. P5 outgoing laser link loss, with possible values loss/no loss.

Not all the 32 combinations of values for the five different binary properties P1-5 are possible. The ones that can be experimentally found and are feasible are reported in Table 2.

The S2 state corresponds to a scenario where another spacecraft is hit by a meteoroid, say spacecraft SC2, and starts rotating, breaking at some point the laser link.

Table 2. LISA States

State ID	P1	P2	P3	P4	P5
S0	conv.	conv.	conv.	no loss	no loss
S1	conv.	conv.	conv.	no loss	loss
S2	conv.	conv.	conv.	loss	no loss
S3	conv.	conv.	conv.	loss	loss
S4	conv.	conv.	div.	loss	loss
S5	div.	div.	div.	loss	loss

conv. = convergent; div. = divergent

In this case, it is possible for SC1 to lose the incoming laser link (the one coming from SC2), without necessarily losing the outgoing one (SC2 could still receive the laser from SC1).

Another important remark is that all the states different from S0 cause an issue: in states S1–3, the SC attitude controller cannot use anymore the high–accuracy DWS sensor that is based on laser links; in states S4 and S5, in addition to the loss of the DWS, the controller itself has to be replaced by a recovery system. From the list of states one can derive all the possible recovery tasks that are needed to cover every possible scenario:

- R1 spacecraft attitude recovery, to be executed in state S5;
- R2 test mass position recovery, to be executed in states S4 and S5;
- R3 incoming laser loss recovery, to be executed in states S3, S4, S5;
- R4 waiting mode, to be executed in state S2.

Of these recovery tasks, only R1 and R2 really require the design of ad-hoc recovery controllers. R3 is simply solved by switching to the star tracker sensor when the incoming laser links are no longer available. Also, R4 is already solved by using the attitude controller developed for R1 and using the internal recovery guidance as the inertial attitude reference.

4.3. Guidance

When at least one of the two incoming laser links are lost, the system relies on the star tracker to provide measurements regarding the spacecraft's attitude. The star tracker can measure the inertial attitude $\mathbf{q}_{SI}$. When the laser sensors are available, they provide directly the attitude error to be fed to an attitude controller, whereas when the star tracker is used, a reference attitude is needed in order to internally compute the angular error.

The reference spacecraft inertial attitude is slowly changing over time, due to the orbit described by the LISA constellation. In this work, the nominal reference attitude was obtained using offline orbital simulations. Specifically, the desired angular velocity $\boldsymbol{\omega}_{CI}$ of the spacecraft is modeled as a sinusoidal function:

$$\text{amplitude of } \boldsymbol{\omega}_{CI} \approx \begin{bmatrix} 1.7266 \cdot 10^{-7} \\ 1.7266 \cdot 10^{-7} \\ -9.9687 \cdot 10^{-8} \end{bmatrix} \text{rad/s} \tag{2}$$

$$\text{pulsation of } \boldsymbol{\omega}_{CI} \approx \begin{bmatrix} 1.9924 \cdot 10^{-7} \\ 1.9924 \cdot 10^{-7} \\ 0 \end{bmatrix} \text{rad/s} \tag{3}$$

$$\text{phase of } \boldsymbol{\omega}_{CI} \approx \frac{\pi}{2} \cdot \begin{bmatrix} 1 \\ 0 \\ 1 \end{bmatrix} \text{rad} \tag{4}$$

The final reference inertial attitude $\mathbf{q}_{ref}$ is computed starting from the inertial attitude at the impact instant $\mathbf{q}_{SI}(t_i)$ and propagating the attitude by means of quaternion kinematics:

$$\begin{gathered} \mathbf{q}_{ref}(t) = \mathbf{q}_{SI}(t_i) \otimes \frac{1}{2} \int_{t_i}^{t} \mathbf{q}_{SI}(\tau) \otimes \mathbf{w}_{CI}(\tau)\, d\tau \\ \mathbf{w}_{CI} = \begin{bmatrix} 0 \\ \boldsymbol{\omega}_{CI} \end{bmatrix} \end{gathered} \tag{5}$$

where $\otimes$ represents the quaternion product.

4.4. Controller

Two controllers are needed to control the spacecraft during the recovery maneuver: a spacecraft attitude controller and a controller for the test mass positions. These two controllers implement respectively recovery tasks R1 and R2.

4.4.1. Spacecraft attitude controller

The general structure of the spacecraft attitude controller is shown in Figure 6. This controller provides the torque command $\boldsymbol{M}_T$ to the spacecraft's MPS system, that schedules the commands to nine independent thrusters in order to apply the requested forces and torques to the spacecraft's center of mass. The controller is based on a proportional derivative control law and takes as input the angular pointing error $\boldsymbol{\theta}_{SC}$. This error can be taken from two different sources: either it is directly provided by the laser sensors (after a simple Euler321 conversion), when these are available, or it is computed by the controller itself.

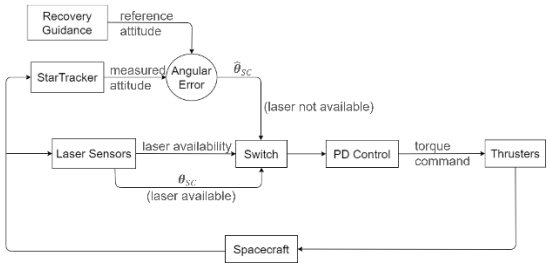

Figure 6. General architecture of the spacecraft attitude recovery controller

When the laser sensors are not available, the angular error is computed as the quaternion error:

$$\mathbf{q}_{err} = \mathbf{q}_{SI}^{*} \otimes \mathbf{q}_{ref} \tag{6}$$

It is possible to feed as input to the PD control law the vector part $\boldsymbol{q}_{err}$ of the error quaternion $\mathbf{q}_{err}$, multiplied by the sign of the scalar part q_{err_0} to avoid the "quaternion unwinding" problem.

A switch changes the source whenever the laser links are reacquired or lost. In general, each spacecraft is equipped with two different sensors that can measure the spacecraft's attitude error: a CAS sensor, with a higher noise, but a larger operating angular range of 250μrad, and a DWS sensor, with a very low noise, but also a very small operating range of 2μrad. The latter is required during the science mode, and has to be available at the end of the recovery maneuver in order to be able to switch back to drag-free control. Finally, when neither the CAS nor the DWS sensors are available, then the star tracker is employed. Overall, the sensor management operates according to the following rules:

- if all the azimuth and elevation angles of the incoming laser beams are smaller than 2μrad, then the DWS is operating and provides $\boldsymbol{\theta}_{SC}$ (after Euler321 conversion from $\mathbf{q}_{SC}$);
- if at least one of the angles exceeds 2μrad, but all angles are below 250μrad, then the CAS is employed, that provides $\boldsymbol{\theta}_{SC}$ (after Euler321 conversion from $\mathbf{q}_{SC}$);
- if all the azimuth and elevation angles are greater than 250μrad, then the star tracker is employed, that provides the spacecraft's inertial attitude $\mathbf{q}_{SI}$.

The final torque command is obtained by the following relationship:

$$\boldsymbol{M}_T = -K_1 \boldsymbol{\theta}_{SC} - K_2 \hat{\boldsymbol{\omega}}_{SC} \tag{7}$$

where $\hat{\boldsymbol{\omega}}_{SC}$ is the estimate of the derivate of $\boldsymbol{\theta}_{SC}$ obtained by filtered differentiation. The filtered differentiation is performed according to the following discrete-time equation:

$$\hat{\boldsymbol{\omega}}_{SC}(k) = N\left(\boldsymbol{\theta}_{SC}(k) - \boldsymbol{\theta}_{SC}(k-1)\right) + (1 - N\tau)\,\hat{\boldsymbol{\omega}}_{SC}(k-1) \quad (8)$$

where N is a tunable constant, that determines the filtering intensity, and $\tau = 0.01$s is the time interval of the filter.

The PD controller has been tuned on the linearized plant of the attitude dynamics extended with actuators and sensing noises. The tuning found is $N = 4$, $K_1 = K_2 = \begin{bmatrix} 800 & 0 & 0 \\ 0 & 800 & 0 \\ 0 & 0 & 1000 \end{bmatrix}$.

4.4.2. Test mass position controller

The general structure of the spacecraft attitude controller is shown in Figure 7. The position of a test mass is controlled by three different PID controllers: the first one provides the force command $\boldsymbol{F}_T$ for the MPS thrusters and takes; the other two control independently the two test masses by means of the electrodes in the test mass housings.

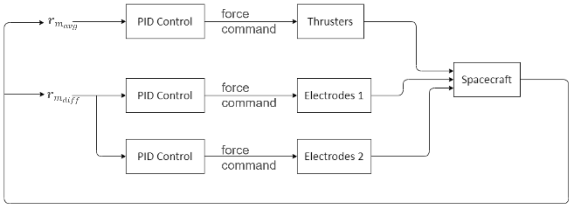

Figure 7. General architecture of the test mass position recovery controller

The controller that provides the force command to the thrusters takes as input the average test mass position $\boldsymbol{r}_{m_{avg}} = \frac{1}{2}\left(\boldsymbol{r}_{m_1} + \boldsymbol{r}_{m_2}\right)$. This recovery action actually moves the spacecraft around the test masses in order to counteract the offset induced by the micrometeoroid impact. The other two controllers act directly on each test mass independently in order to further compensate any residual offset. These take as input the differential test mass position $\boldsymbol{r}_{m_{diff}} = \frac{1}{2}\left(\boldsymbol{r}_{m_1} - \boldsymbol{r}_{m_2}\right)$.

Each PID controller is of dimension 3 by 1 and is defined by the following discrete-time transfer function:

$$P + I \cdot \tau \frac{1}{z-1} + \frac{D}{1 + N\tau \frac{1}{z-1}} \quad (9)$$

where for the first thruster controller $P = [200 \quad 200 \quad 195]$, $I = [2.94 \quad 2.94 \quad 2.54]$, $D = [3847 \quad 3847 \quad 3330]$, $N = 18$ and $\tau = 0.1$s; for the PID controller of test mass 1 $P = -[200 \quad 200 \quad 200]$, $I = -[2 \quad 2 \quad 2]$, $D = -[3500 \quad 3500 \quad 3500]$, $N = 18$ and $\tau = 0.01$s; for the PID controller of test mass 2 $P = [200 \quad 200 \quad 200]$, $I = [2 \quad 2 \quad 2]$, $D = [3500 \quad 3500 \quad 3500]$, $N = 18$ and $\tau = 0.01$s.

All the tuning parameters have been obtained by means of the Simulink PID Autotuner by setting maximum robustness and response speed.

5. Simulation Results

A Monte Carlo simulation campaign has been performed to assess the effectiveness of the proposed solution, where 100 of the strongest impacts available in the ESA dataset have been simulated. To better quantify the obtained performance, three parameters have been used:

1. Percentage of successful recoveries (PSR);
2. Recovery time needed to complete the recovery maneuver (RET);
3. Maximum absolute angular error for each of the three axis (MAX).

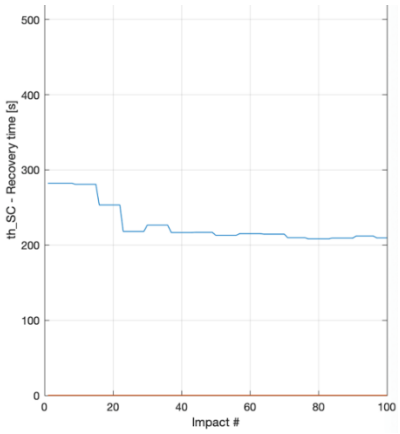

Figure 8. RET performance index

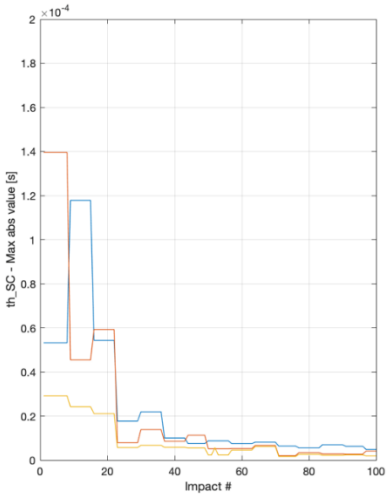

Figure 9. MAX performance index

The obtained PSR is 100% and, as shown in Figure 8 and Figure 9, the recovery system has proven to be effective in the recovery task. In particular, the

recovery time is always below 300s, that is a significant reduction with respect to the average time required by the complete link reacquisition maneuver (several hours).

6. Conclusions

In this paper, a preliminary analysis of the impact data has been first carried out in order to gain insight about the possible states of the LISA system in the case of a micrometeoroid impact. The LISA system operating modes has been modeled using a state machine and the main recovery tasks have been defined. Then, a possible recovery system has been developed, based on several PD/PID controllers. Finally, the results of a Monte Carlo campaign have been shown, demonstrating the effectiveness of the proposed strategy.

Acknowledgements

This work was supported by ESA/ESTEC. The view expressed in this work cannot be taken as the official position of the European Space Agency.

References

[1] P. Amaro-Seoane et al., Laser Interferometer Space Antenna, arXiv e-prints, p. arXiv:1702.00786, 2017.
[2] ESA, LISA Yellow Book, Assessment Study Report, 2011.
[3] Vidano, C. Novara, L. Colangelo, J. Grzymisch, "The LISA DFACS: a Nonlinear Model for the Spacecraft Dynamics", Aerospace Science and Technology 107 (2020) ISSN 1270-9638.
[4] J.I. Thorpe et al., "LISA Pathfinder as a Micrometeoroid Instrument", Journal of Physics: Conference Series 840 (2017).
[5] J.I. Thorpe et al., "Micrometeoroid Events in LISA Pathfinder", The Astrophysical Journal 883 (2019).
[6] S. Vidano, C. Novara, J. Grzymisch, M. Pagone, "The LISA DFACS: Overview of the Control Design Activities for the Drag-Free Mode", 11th ESA Guidance Navigation and Control Conference, Virtual, 2021, 22-25 June.